Minerals Engineering 213 (2024) 108746

Contents lists available at ScienceDirect

Minerals Engineering

journal homepage: www.elsevier.com/locate/mineng

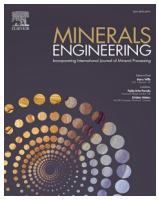

# Three-dimensional characterization of porosity in iron ore pellets: A comprehensive study

Pasquale Cavaliere [a,*], Behzad Sadeghi [a], Leandro Dijon [b], Aleksandra Laska [c], Damian Koszelow [d]

[a] Department of Innovation Engineering, University of Salento, Via per Arnesano, 73100 Lecce, Italy
[b] VALE, Route de Pallatex 29 St-Prex, 1162 Losanna, Switzerland
[c] Faculty of Mechanical Engineering and Ship Technology, Gdansk University of Technology, Narutowicza 11/12, 80-233 Gdańsk, Poland
[d] Advanced Materials Centre, Faculty of Electronics, Telecommunications and Informatics, Gdańsk University of Technology, 80-233 Gdańsk, Poland

ARTICLE INFO

*Keywords:*
Hydrogen
Direct reduced iron
Microtomography
Porosity
Re-oxidation

ABSTRACT

This paper presents a comprehensive study on the production and reduction of high-quality iron ore pellets characterized by a basicity index nearing 0.5 and diameters ranging from 1 to 2 cm. The reduction process was carried out in a hydrogen atmosphere at temperatures spanning 800–1000 °C and a pressure of 8 bar. Initial findings revealed substantial variations in pellet density and compressive strength, attributed to their mean dimensions. To delve into the microstructural transformations occurring during reduction, meticulous micro-tomographic analyses were conducted on each pellet before and after the reduction process. The research assessed reducibility factors such as porosity, pore size, and tortuosity adjustments across diverse reduction conditions. The study highlights the intimate connection between the reduction process rate, processing parameters, and pellet microstructure. Furthermore, the metallization tendencies were explored through extensive reduction experiments involving multiple pellets. These findings offer crucial insights into optimizing iron ore pellet performance during production and reduction processes, contributing to advancements in industrial applications.

## 1. Introduction

Iron ore and steel products are essential components of modern society, and their production efficiency is critical for sustainable development. In the steelmaking process, iron ore undergoes reduction to become primary iron, which is further refined to yield the final product. Before entering the steelmaking phase, iron ore must undergo several processing steps to eliminate impurities, increase concentration, and modify granulometry (Cavaliere, 2019). During this process, the ore is categorized into three granulometry types: granulated ore, with a size ranging from 31.0 to 6.3 mm; sinter feed, sized between 0.15 mm and 6.3 mm; and pellet feed, with a granulometry below 0.15 mm (Biswas et al., 2023). The granulated ore requires suitable granulometry for furnace reduction, whereas sinter feed and pellet feed, being fine ore fractions, cannot be directly used due to potential furnace clogging and gas transport impediments (Mohammad et al., 2023).

For a long time, the coarse ore fraction was loaded into blast furnaces, while the fine fraction accumulated in piles without economic value. To make use of this ore fraction, agglomeration technologies such as sintering and pelletizing were developed. These processes shape the material into the required form and size (usually several centimeters for sinter and approximately 12 mm, with variations from 10-16 mm, for pellets) (Reddy et al., 2023). Consequently, the iron ore charge for blast furnaces can comprise a mixture of ore lump, iron ore sinter, and iron ore pellets. The pellet manufacturing process involves three main stages: raw material preparation, raw pellet formation, and pellet hardening through heat treatment (Zhang et al., 2023). The final product should possess porosity to enhance heat transfer and facilitate the reduction process while maintaining mechanical strength (Cavaliere et al., 2023; Cavaliere et al., 2023; Cavaliere et al., 2023). Achieving the right balance between reducibility and strength is crucial in assessing pellet quality. Reducibility refers to the ability of the pellets to be reduced to metallic iron in the blast furnace, while strength refers to the ability of the pellets to withstand mechanical stresses during handling and transportation (Metolina et al., 2023).

Iron ore pellets, alongside lump ore and sinter, are fundamental raw

* Corresponding author.
*E-mail address:* pasquale.cavaliere@unisalento.it (P. Cavaliere).

https://doi.org/10.1016/j.mineng.2024.108746
Received 19 October 2023; Received in revised form 17 May 2024; Accepted 18 May 2024
Available online 24 May 2024

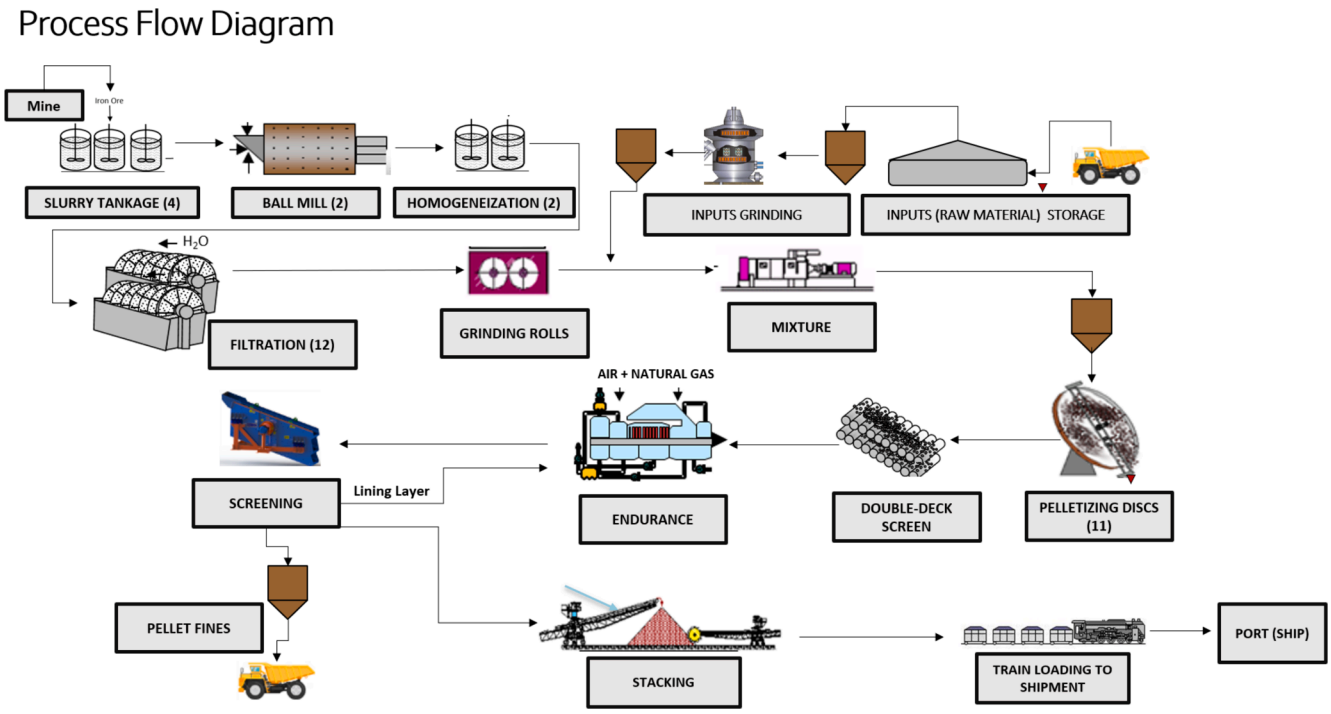


**Fig. 1.** Pellets production flow diagram.

materials for steel production, generated through the pelletizing process (Singh et al., 2023). The porosity developed during pellet manufacturing is a critical attribute. It enables internal gas flow, enhancing reducibility and process efficiency (Kim and Sohn, 2023). Nevertheless, porosity also impacts the physical integrity of the pellets, which must endure various stresses during handling, transportation, and processing. Thus, the quantity, size, shape, and distribution of pores are essential aspects of pellet quality control. Traditionally, porosity characterization relied on techniques like mercury intrusion porosimetry (PIM) and optical microscopy (OM) (Korobeinikov et al., 2023; Zhang et al., 2023). PIM, however, solely assesses surface-connected pores, while OM is confined to two-dimensional space, potentially yielding unrepresentative data.

To overcome the limitations of PIM and OM, recent advancements in technology have introduced more sophisticated methods for porosity characterization. One such method is X-ray microtomography (micro-CT), which allows for a non-destructive three-dimensional analysis of the internal structure of iron ore pellets. This technique provides a comprehensive understanding of the pore network, including the connectivity and tortuosity of the pores (Ju et al., 2023). Furthermore, micro-CT can quantify the size, shape, and distribution of pores with high accuracy, thereby offering a more reliable assessment of pellet quality.

In addition to micro-CT, computational modeling and simulation techniques are also being employed to predict the behavior of iron ore pellets under various conditions (Augusto et al., 2015; Ljung, 2010). These models take into account the physical and chemical properties of the pellets, as well as the environmental conditions during handling, transportation, and processing. By simulating these conditions, researchers can optimize the pellet manufacturing process to achieve the desired porosity while maintaining the physical integrity of the pellets. Recent advances have seen the application of MicroCT-based porosity characterization, offering three-dimensional insights into iron ore pellets. MicroCT, a form of 3D microscopy, provides comprehensive internal and external structural information without extensive sample preparation (Tang et al., 2023). Thus, our aim is to develop a porosity characterization methodology for iron ore pellets, potentially complementing or replacing conventional techniques. We acknowledge the limitations of each approach (Bezerra and Augusto, 2020).

To obtain primary iron, two commercially viable production routes exist: blast furnace reduction, yielding liquid pig iron, and direct reduction, which produces solid iron sponge or DRI (direct reduced iron) (Cavaliere, 2019; Cavaliere, 2019). DRI encompasses metallized products derived from the solid-state reduction of iron ore (granules and pellets) in direct reduction reactors (Nurdiawati et al., 2023). DRI is primarily composed of metallic iron, residual iron oxides, and reactor contaminants such as silica, alumina, and calcium. DRI reoxidation, particularly during storage and transport, presents ignition risks, requiring specialized handling as water is ineffective for extinguishing reoxidation-induced fires (Bersenev et al., 2022; Li et al., 2021). Certain pellets exhibit a greater propensity for self-ignition during direct reduction, likely due to altered process conditions (Yazir et al., 2021; Hamadeh et al., 2018). Despite these observations, current laboratory test methodologies, standardized by ISO, do not adequately address this behavior or provide insights into predicting autoignition occurrences (Anameric and Kawatra, 2007). In direct reduction, iron oxides are solid-state reduced to metallic iron without melting, resulting in increased porosity and fine generation (Pfeiffer et al., 2023). The removal of oxygen leaves a highly porous structure (Meshram et al., 2022; Man and Feng, 2016), and both raw materials and reduction temperature influence DRI porosity (Cavaliere et al., 2023; Cavaliere et al., 2023; Cavaliere et al., 2023).

Despite these technological advancements, challenges remain in accurately characterizing and controlling porosity in iron ore pellets. In addition, the heterogeneous nature of these materials hinders complete description through stereological methods (Shen et al., 2023). This study is aimed to propose a three-dimensional porosity characterization methodology for iron ore pellets, leveraging X-ray microtomography (MicroCT) and image analysis to study open and closed pores separately. Factors such as predominant phase fractions, pore distribution, morphology, and phase connectivity are pivotal in understanding pellet behavior during the process (Ju et al., 2023).

This study aims to develop a three-dimensional porosity characterization methodology for iron ore pellets, enabling the separate study of open and closed porosity. We seek to compare the results with classical

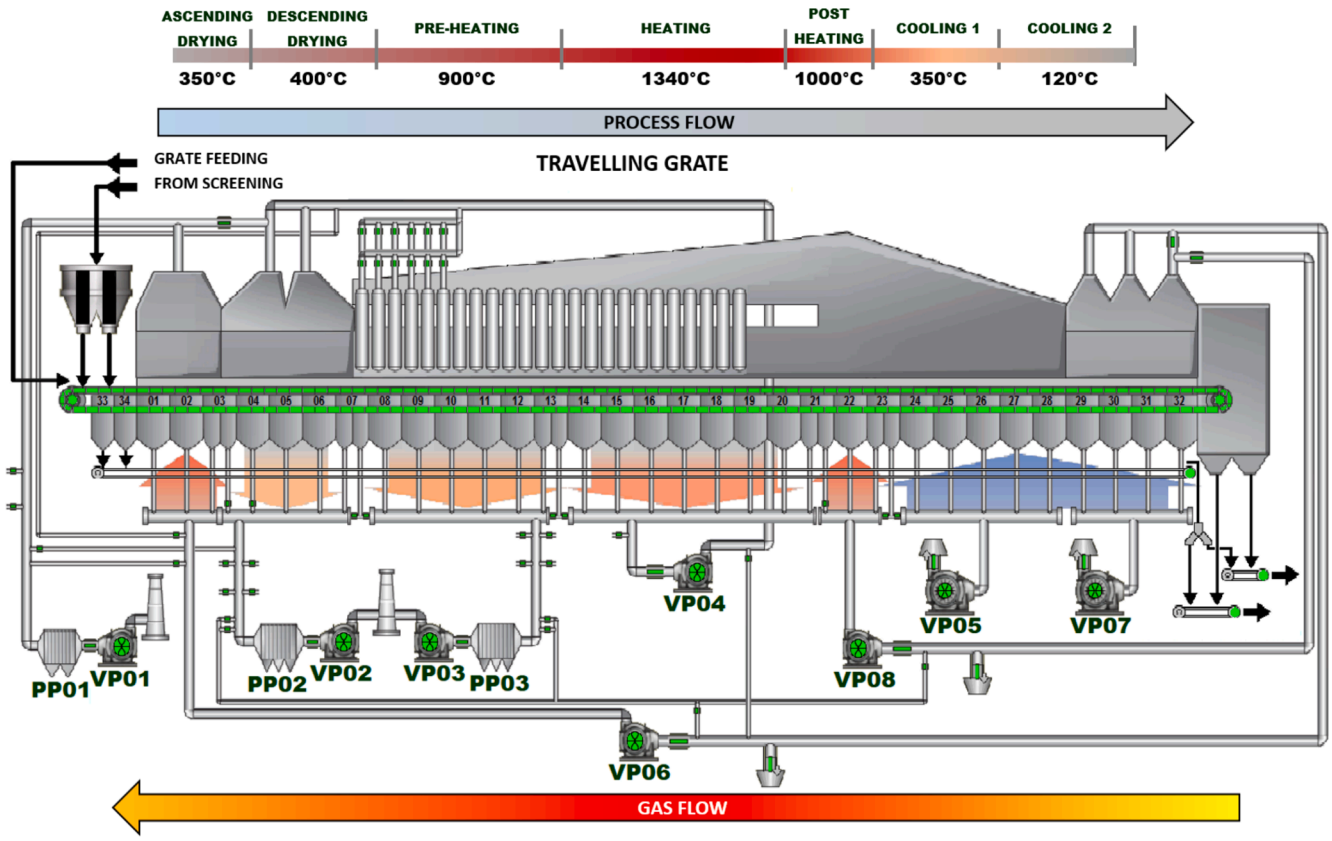


**Fig. 2.** Endurance procedure schematic with (in scale) the indication of the different stage temperatures. PP = Precipitator, VP = Vacuum Pump.

**Fig. 3.** Customized shaft furnace.

porosimetry techniques, especially in assessing porosity evolution and pore geometry during direct reduction in a hydrogen atmosphere. Our methodology involves acquiring MicroCT images of iron ore pellets in different geometric configurations, comparing lower and higher resolutions, and subsequently processing and analyzing these images for qualitative and quantitative material assessment.

## 2. Experimental procedure

### 2.1. Mining and pelletizing procedure

The examined pellets were supplied by VALE (Brazil), and the pelletization process is illustrated in Fig. 1.

The iron ore pelletizing plant starts with the grinding stage, where the ore is combined with a precise solid content and grinding balls of different sizes. The plant is equipped with several ball mills, each of which has a considerable capacity for processing the ore. The most important quality parameter at this stage is the specific surface area (Blaine), which is usually in the range of 1,500 to 1,600 $cm^2/g$. After the grinding process is completed, the material passes through vacuum filtration. The filters used in this stage are characterized by their large diameter and provide a large filtration area. After the filtration stage, the material undergoes a treatment with high pressure grinding rolls (HPGR), which further improves the quality parameters. The HPGR process is characterized by its capacity and uses rollers with specific dimensions in terms of diameter and width.

The material is then fed to the pelletizing discs, with each disc providing a different capacity. The plant has several discs, and both the discs and the screens have specific dimensions in terms of their diameter and width. Finally, the material is subjected to a continuous treatment, as shown in Fig. 2.

At the end, the pellets go through a filtration step to remove fines less than 5 mm. This thorough process culminates in the production of iron

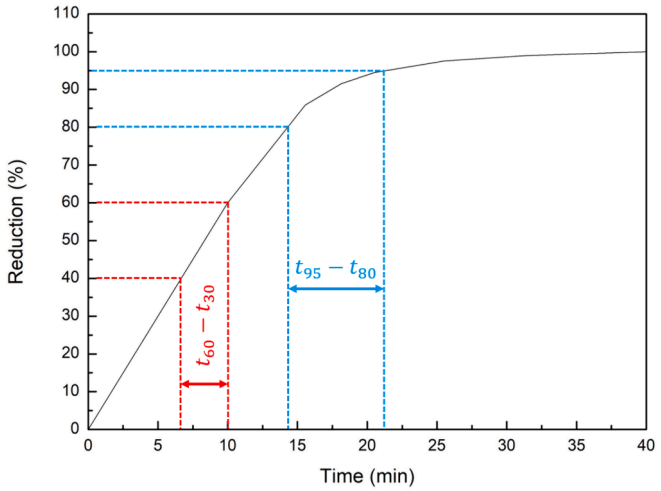


**Fig. 4.** Rates of reduction indexes calculation.

ore pellets, which serve as an important resource for various industries.

### 2.2. Characterization procedure

The composition of the pellets was studied by energy dispersive X-ray spectroscopy (EDS) in a Zeiss EVO 60 scanning electron microscope. To determine pellet density, seven pellet diameters were measured and the average diameter was calculated. Subsequently, this average diameter was employed to calculate the pellet density by weighing the pellets accurately using a balance with a resolution of 0.0001 g. The pellets were then weighed with a balance. In addition, the surface microstructure of the pellets was examined using a scanning electron microscope (SEM) to quantify the surface pores. The compressive strength of the pellets was measured using a Zwick/Roell Z100 standard testing machine at a speed of 0.5 mm/min (the example movie of the performed tests is shown in Supplementary Material). A specially designed shaft furnace was used for the comminution experiments of the pellets, which is shown in Fig. 3.

### 2.3. The gas composition was 100 % H2 hydrogen

From the reduction curves, which represent the percentage of reduction versus time to reduction, we calculated the kinetics constants and the reduction rates. The kinetic constant was calculated through the three dimensional diffusion model (Eq.1):

$$k = \frac{[1-(1-\alpha)^{\frac{1}{3}}]^2}{t} \quad (1)$$

and through the three dimensional phase boundary controlled reaction (Eq.2):

$$k = \frac{1-(1-\alpha)^{\frac{1}{3}}}{t} \quad (2)$$

where α is the fraction reacted (0–1) and t is the time at which a given fraction of the material reacts (Man and Feng, 2016).

The reduction rate is analyzed through the definition of two indexes described in Equations 3 and 4:

$$\frac{dR}{dt}_{40} = \frac{33.6}{t_{60} - t_{30}} \quad (4)$$

$$\frac{dR}{dt}_{90} = \frac{13.9}{t_{95} - t_{80}} \quad (5)$$

with $t_{95}$, $t_{80}$, $t_{60}$ and $t_{30}$ being the time required to reduce the pellets by 95, 80, 60 and 30 %. This is schematized in Fig. 4.

The morphology and evolution of particle pores were analyzed by microtomography using General Electric's Phoenix v/tome/xs system. Microtomography data were then analyzed using Image J software to characterize the porosity of the material. Selected pellets were completely metallized during the reduction process and then reheated in a heat treatment furnace at 200 °C to 700 °C for different times to determine their reoxidation behavior. All CT scans were performed at 150 kV and 10 W, with the sample rotated 360° during imaging. Factors such as exposure time and number of projections directly affect the overall analysis time. Binding is a process that involves grouping pixels, which also affects analysis time; It increases the signal-to-noise ratio but

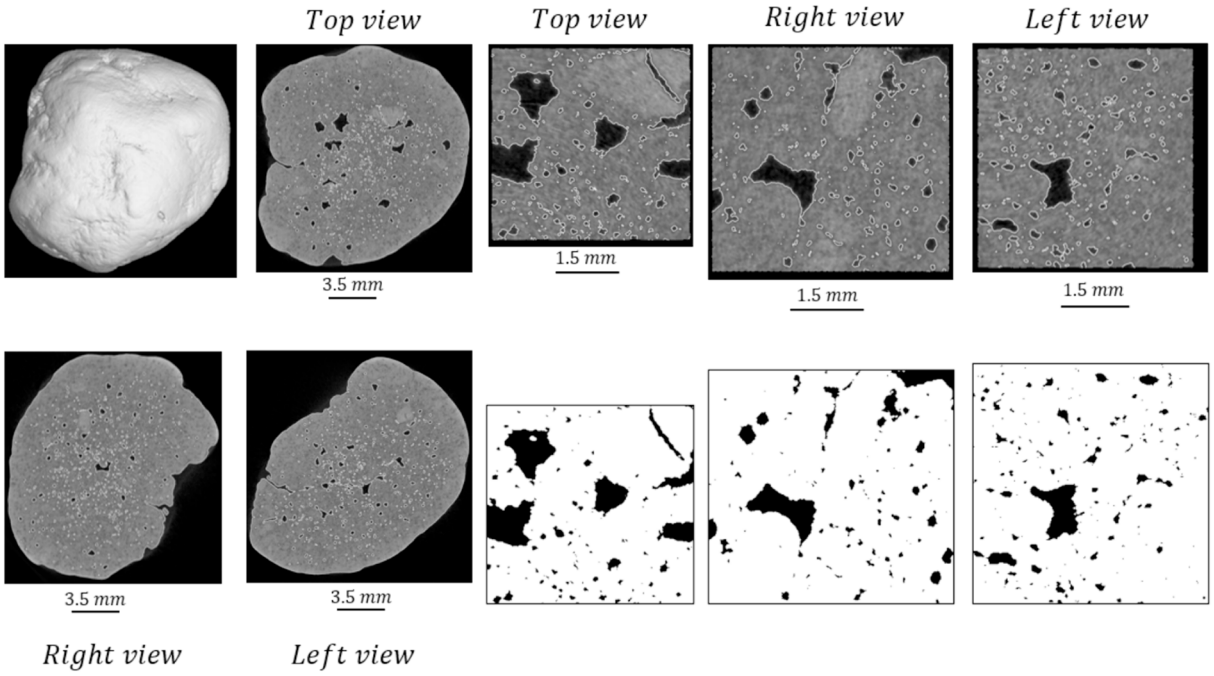


**Fig. 5.** Tomography analyses example performed on the studied pellets.

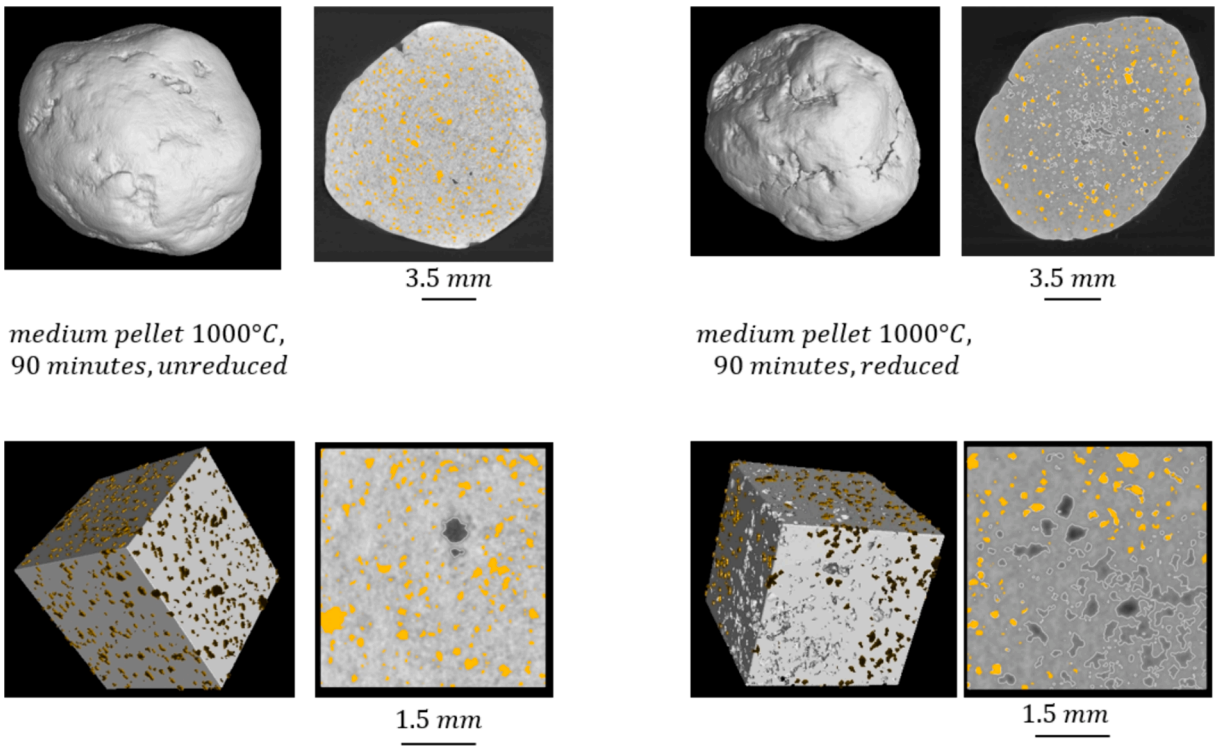


**Fig. 6.** Pellets structure analysed selecting different volumes sections.

reduces the resolution, thus affecting the pixel size.

In all acquisition processes, a filter type suitable for the analysis of dense samples requiring high energy products is used. Filters are used to eliminate lower-energy X-rays that would otherwise be preferentially absorbed near the surface of the sample. This selective absorption, known as beam hardening, can generate artifacts that degrade the image quality, making the edges of the sample appear denser. The choice of filter was based on the transmission value, which is a ratio between the X-ray signal received with the sample and without the sample. For image preprocessing, open-source software FIJI/ImageJ was used. In an effort to optimize analysis conditions with respect to image quality and acquisition time, various parameters were experimented with, including different geometric configurations during acquisition, which inherently altered image resolution, as well as reductions in the number of projections and the angular range of sample rotation, from the standard 360° to 180°.

## 3. Results and discussion

X-ray microtomography was used to analyze the pellets. Pellets were classified into three groups based on their mean diameter: small (up to 1.1 cm), medium (1.1 to 1.5 cm), and large (with a diameter greater than 1.5 mm). Individual pellet reduction tests were performed, with reduction times set at 5 min, 30 min, and 90 min, to follow the evolution of porosity. Various parameters were calculated, including the variation of porosity and tortuosity under different reduction conditions for each individual pellet. All tomography images of the monitored pellets are included in the Supplementary Material, which can be accessed via an online link. X-ray computed microtomography is a nondestructive technique that allows internal and three-dimensional visualization of a sample exposed to ionizing radiation and requires minimal physical and chemical sample preparation (Nie et al., 2023). It works on the same principle as conventional radiography, where different parts of a sample absorb radiation to different degrees. Consequently, it allows the nondestructive examination of two-dimensional cross sections, which can be reconstructed using mathematical principles to create a corresponding three-dimensional model of the sample. This in turn allows visualization and quantification of the internal structure of the material (El-Zoka et al., 2023). Computed tomography produces an image that closely approximates reality by displaying the average attenuation of each small volume element, ordering the attenuation data, and providing quantitative information, as shown in Fig. 5.

After the post-processing step, the image finally goes to the attribute extraction in which the quantitative data of interest are obtained (Fig. 6).

The numerical data contained in the images can be acquired and analysed, allowing subsequent steps of classification and pattern recognition. Pore segmentation was performed using the freely available software FIJI /ImageJ. A lower threshold was determined visually to exclude some pores from selection, and an upper threshold was set above which non-filled pores were selected, but also above which segmentation of solid partial remnants began. This threshold (either maximum or minimum) was consistently applied to all sample layers. The determination of this threshold is of critical importance, as it significantly affects the calculation of the porosity fraction in iron ore pellets. The images have well-defined contrast, which allows better segmentation of tonal variations. To distinguish between open and closed porosity, a novel pore discrimination method based on the calculation of Euclidean distances (EMD) was used to delineate the pellet edge (Ignacio et al., 2022). The minimum edge distance (MDE) of the filled object provides a hue reference where each object is assigned a hue based on its distance from the pixel to the object edge. The lowest hue values are related to connected pores, since this type of pore is in contact with the edge. Consequently, after calculating the MDE, a graph of minimum intensity is created, with the smallest values corresponding to connected pores.

Segmentation is done interactively by applying a fixed threshold to each 2D layer of the model. The selection of the separation cutoff tone value affects the number of pixels. To determine the porosity percentage and segmentation of iron ore pellet images was still difficult even after all previous steps, we used five different segmentation thresholds for each sample, with a difference of 5 tons between them. Then,

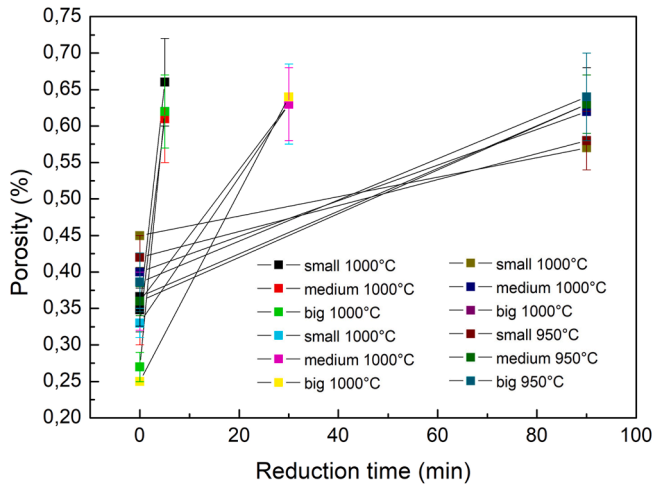


**Fig. 7.** Porosity as a function of temperature and reduction time for different size pellets.

segmentation is performed using these values and the pore volume is subtracted for each volume obtained. Therefore, the estimated value of the porosity of each sample falls within the scope of determining these thresholds (Wei et al., 2019).

Porosity is generally the rate limiting step of the reduction process (Fig. 7).

Pores in materials can be grouped based on how easily they can be reached by outside fluids. Closed pores are entirely isolated from external fluids and other pores, influencing macroscopic properties like density, elasticity, mechanical strength, and thermal conductivity. However, they are irrelevant in processes involving fluid flow and gas adsorption. Pores that have a communication channel with the external surface of the solid are referred to as open pores (Mishra, 2020). Open pores have various designations, including "pore-through," which features an open channel starting at one point on the surface, passing through the particle, and emerging at another surface location. Another type is "blind-pores," which have an opening at only one end. Pores with slight surface irregularities are technically considered blind-pores, but it's better to treat them separately as a distinct characteristic known as surface roughness (Yi et al., 2013).

The main factor influencing the process is the porosity of the pellets in terms of dimensions, tortuosity, and pore distribution (Ghadi et al., 2016). This is closely related to the specific volume of hydrogen reacting with the pellet's internal surface. In cases of low porosity and small surface pore dimensions, gas encounters numerous obstacles in penetrating the pellet. Consequently, solid-state diffusion from the surface becomes more significant but operates at orders of magnitude slower rates than gas diffusion. As a result, all chemical reactions are driven by hydrogen adsorbed on the pellet surface (Ma et al., 2021).

This aspect is crucial for the swelling behavior of pellets within industrial reactors (Huang et al., 2012). In fact, porosity and pore dimensions significantly affect the kinetics of direct reduction, and when porosity decreases due to pellet compression within DRI reactors, the time required for complete reduction is substantially prolonged (Ghadi et al., 2023). Therefore, the microstructural characteristics of iron ore pellets play a pivotal role in evaluating factors that influence their behavior during reduction processes. Porosity, for instance, must be adequate to enable gas flow, enhancing process efficiency, without sacrificing mechanical strength, essential for transportation and handling. Thus, the distribution of pore size and shape are vital aspects of pellet properties. The volumetric fraction and morphology of each phase present also contribute to the pellets' metallurgical quality (Lei et al., 2023). Conversely, resistance increases with decreasing porosity. To achieve both high strength and high reducibility at the same time, a potential solution is to produce pellets with open pore structures or closed pores near the surface but with low overall porosity (Rao et al., 2023).

Porosity tends to increase as the reduction processes take place Fig. 8).

As the reduction process progresses, this phenomenon tends to speed up the reaction rate. Considering that diffusion can often be the limiting step, porosity and pore dimensions have a significant impact on the reduction process (Zheng et al., 2023). This is because both porosity and

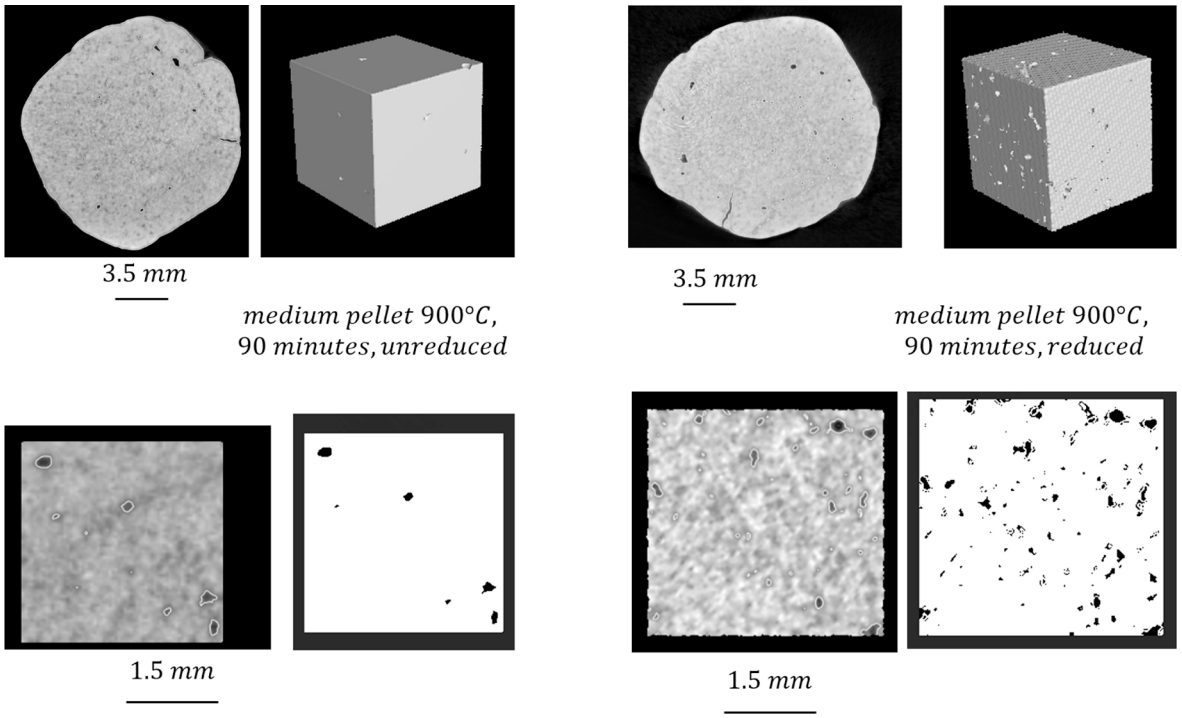


**Fig. 8.** Porosity analyses for selected pellets.

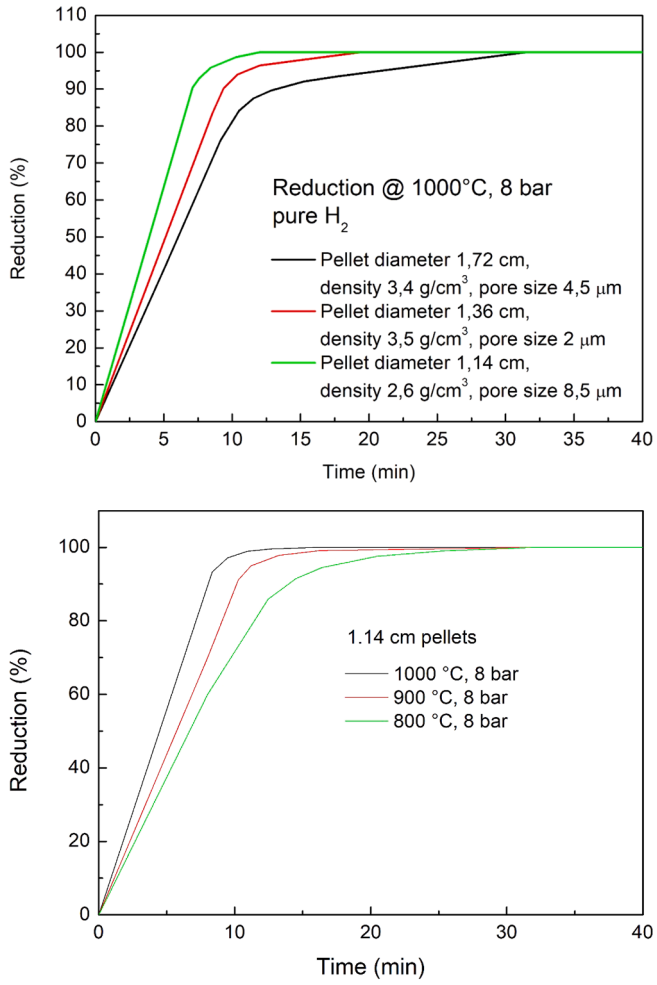


**Fig. 9.** Reduction curves for selected pellets.

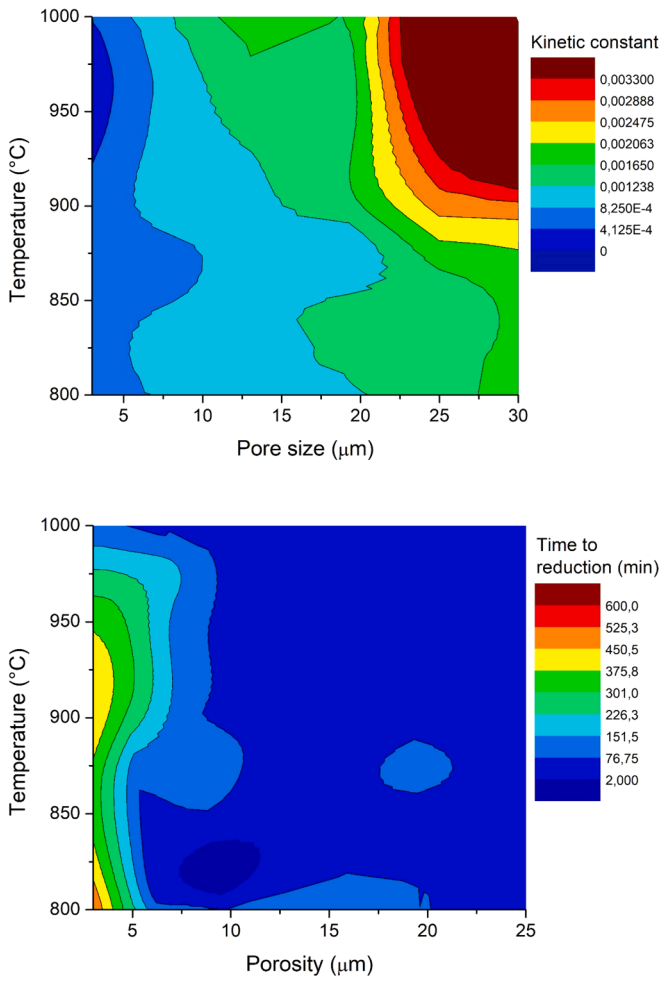


**Fig. 10.** Kinetic constant and time to reduction as a function of the most influencing parameters.

pore size determine the specific surface area of the pellets, thus defining the available surface for reaction development. This aspect is crucial and needs to be accurately included in a model that can effectively describe how these systems evolve (Lyu et al., 2023).

Entropy generation arises from two main factors: chemical reactions and mass transfer. When we analyze these factors individually, we observe that as the porosity of the pellet decreases, entropy generation caused by heat transfer increases (Bai et al., 2022). In this situation, entropy rapidly increases during the initial stages of reduction because of the temperature difference between the pellet surface and the heated hydrogen. Afterward, entropy decreases and reaches a stable state as the temperature gradient diminishes during the progression of the reduction process (Rukini et al., 2022).

On the other hand, when we consider pellets with increasing porosity, the resistance to gas penetration inside the pellets decreases. Consequently, entropy generation due to gas flow decreases. The second contribution pertains to entropy generation from chemical reactions. In this case, entropy generation tends to rise rapidly during the initial reaction stages but then decreases to zero as the chemical reactions progress (Li et al., 2023). Here as well, an increase in pellet porosity leads to a decrease in entropy generation. It's important to note that entropy generation results in increased energy consumption for the overall reduction process.

An example of the reduction curves in some experimented conditions is shown in Fig. 9.

As a matter of fact, Fig. 10 shows the results of the reduction behaviour as a function of temperature and pores size for the studied high-grade pellets.

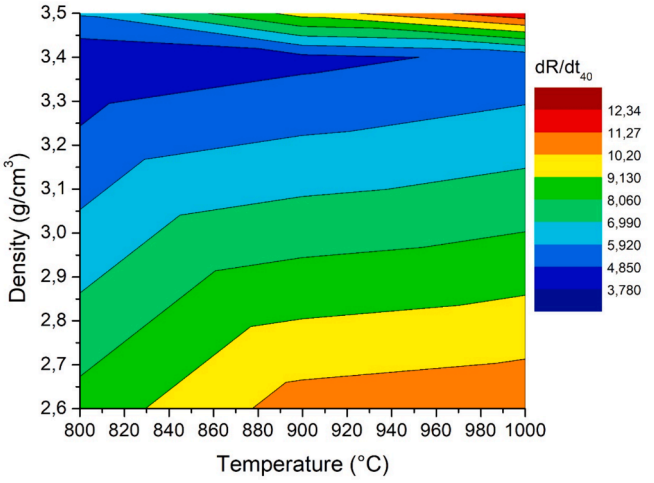


**Fig. 11.** dR/dt40 index as a function of reduction temperature and pellets density.

The kinetics of reduction are significantly accelerated as the dimensions of the pores increase, regardless of the temperature. In other words, larger pores lead to faster pellet reduction. The reduction reactions of high-density pellets progress stepwise, which can be described using a shrinking core model. On the contrary, for low-density pellets,

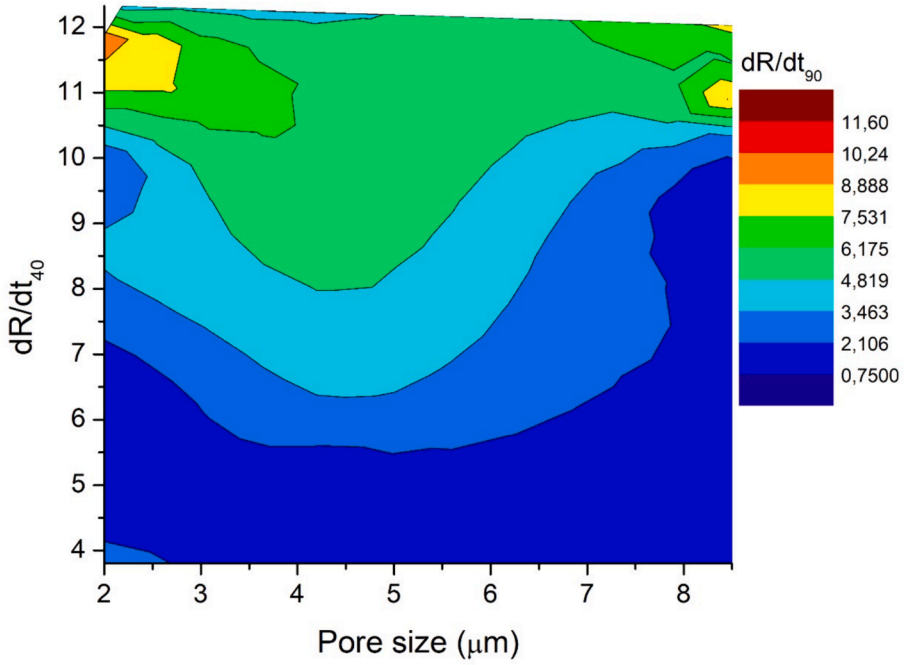


**Fig. 12.** dR/dt90 as a function of pore size and dR/dt40.

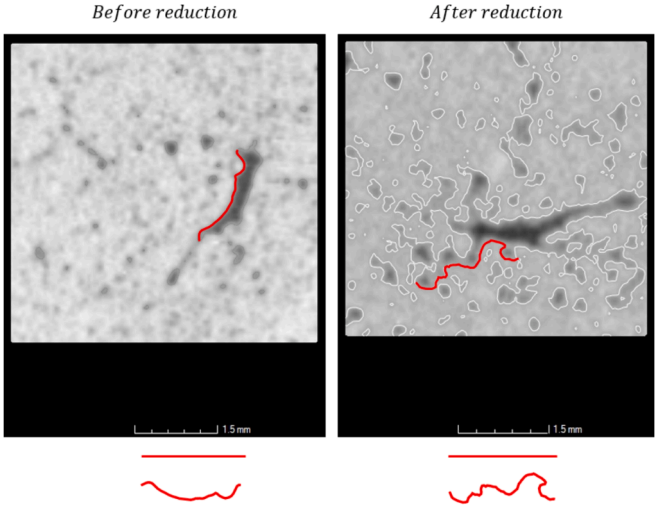


**Fig. 13.** Small pellet before reduction and after reduction at 1000 °C for 90 min.

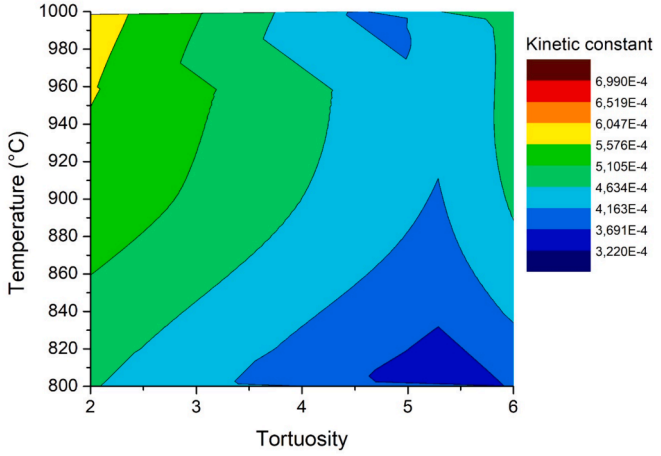


**Fig. 14.** Kinetic constant as a function of reduction temperature and pores tortuosity.

gas diffusion occurs very rapidly, resulting in significantly reduced reduction times. Therefore, the time required for reduction is shorter for low-density pellets, which in this specific scenario are also characterized by intermediate surface pore dimensions.

The contribution to entropy generation from mass transfer is another significant factor in the reduction process. Highly porous pellets can approach zero entropy generation due to enhanced gas penetration inside the pellets. However, entropy is never null because of the compositional gradient between the pellet surface and the yet-to-be-reduced core. Heat transfer has the most significant effect on entropy generation, followed by chemical reactions, while mass transfer has the smallest impact. During the initial stages of reduction, both chemical reactions and gas diffusion control the process, while in the later stages, the rate-limiting step becomes the interfacial chemical reactions. The calculation of the dR/dt40 index is typically used to assess the first (rapid) stage of reduction. This index is highly dependent on pellet density, as illustrated in Fig. 11.

Pellets with very small surface pores and a denser surface, typically seen in medium-sized pellets, develop a robust iron layer on the surface during reduction. This dense and hard iron layer has a significant adverse effect on the reduction rate. the development of a dense and hard iron layer during reduction has a significant adverse effect on the reduction rate of pellets with very small surface pores and a denser surface. Gas penetration through these hard iron layers can be enhanced at higher temperatures, but this can lead to softening of the pellets, reducing their porosity and affecting reduction rates. The final reduction stage of the overall process is typically assessed using the dR/dt90 index as depicted in Fig. 12.

As already observed, the pores aspect strongly varies during reduction.

As porosity increases, the dimensions of individual pores also increase, and the tortuosity of the pores varies, as illustrated in Fig. 13. Consequently, tortuosity tends to continuously change during the

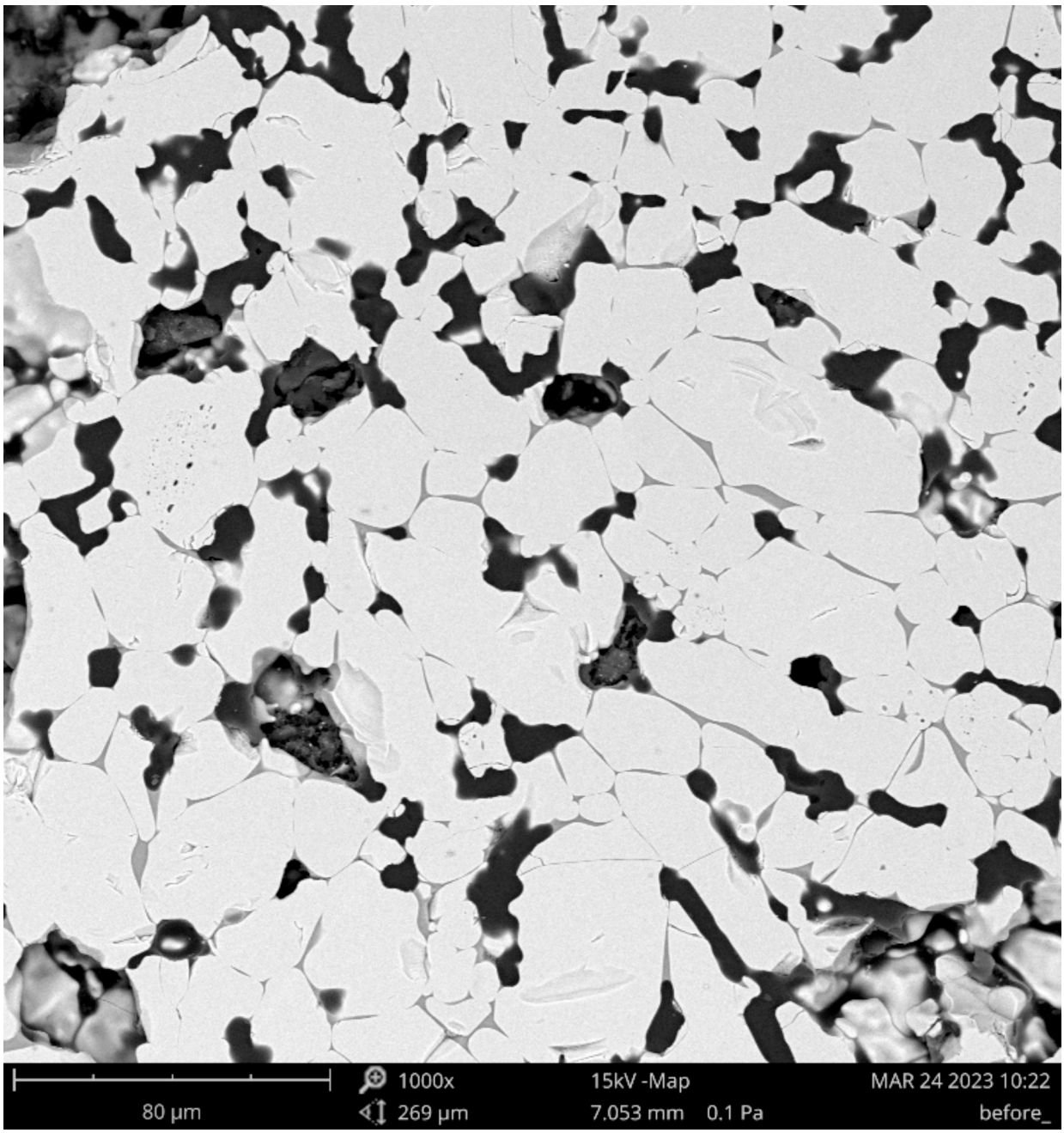


**Fig. 15.** SEM microstructure of the pellets before reduction.

reduction process. The initial value of tortuosity and its variation during reduction have a notable impact on pellet kinetics. The general behavior of reduction kinetics as a function of temperature and pore tortuosity is presented in Fig. 14.

Tortuosity delays the reduction process for a given temperature. As tortuosity increases, the turbulence of gas flowing within the pores also increases, leading to a decrease in the reduction rate. Under such conditions, the reduction rate tends to decrease. Considering the tortuosity factor within the pellets, The time required for reduction increases as pore tortuosity increases, porosity decreases (resulting in increased density), and pore dimensions decrease. These parameters significantly contribute to variations in entropy generated throughout all the reduction phases.

Entropy begins to increase in the initial stages of direct reduction due to heat transfer between the heated hydrogen and the pellet surface. Entropy continues to rise as porosity and the gas ratio decrease due to reduced exchange surfaces. Further increases in entropy generation occur as pore tortuosity increases (Sundberg, 2021). Tortuosity acts as an obstacle to gas flow and its ideal path within the pellet, thereby reducing overall gas diffusion and its reduction effect (Ali et al., 2022). Tortuosity has substantial implications for overall entropy behavior and energy input during the direct reduction process. Additionally, tortuosity has a greater impact as pellet diameter increases. As tortuosity increases, both entropy generation and energy consumption increase (Gautam and Cole, 2022; Singh et al., 2022), and entropy generation tends to exhibit a nonlinear behavior, particularly in the final stages of reduction when pellet tortuosity is highly pronounced. The microstructural analyses of the pellets evolution was performed through SEM and microanalyses (Fig. 15).

Based on our previous studies, we have found that the basicity index

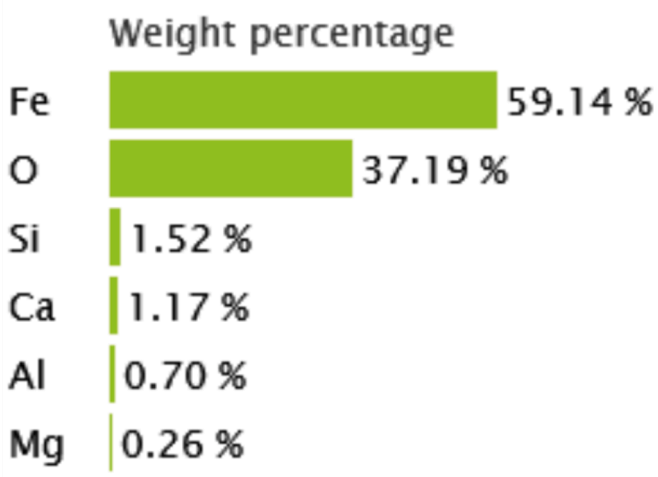


**Fig. 15.** (*continued*).

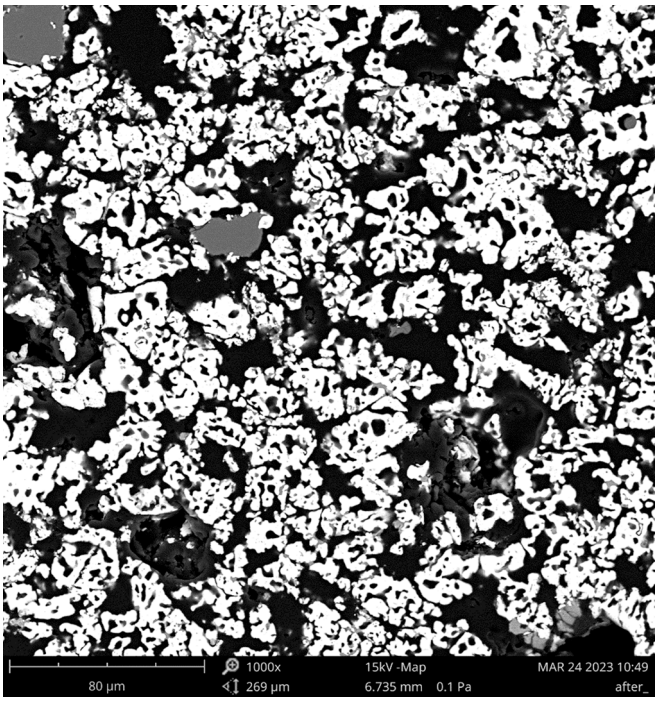


**Fig. 16.** SEM microstructure after reduction at 1000 °C for 30 min.

plays a crucial role in accelerating reduction reactions. However, the relationship between reduction behavior and the basicity index is complex. Experimental evidence has shown that reduction kinetics tend to increase as the basicity index varies from 0 to 1, but then it begins to decrease again as the basicity index increases. This suggests a parabolic relationship between the time required for reduction and the basicity index. Therefore, the reduction behavior of industrial pellets is closely tied to the quality of the raw material, which in turn influences the process and the quality of the final product for subsequent operations. Maintaining the basicity index at an appropriate level is essential for optimizing the pellet reduction process. This effect is more pronounced when there is a higher presence of CaO in the pellet composition. An excessive amount of CaO can make the produced pellets overly brittle, making them challenging to handle in subsequent processing operations. In our observations, hematite predominates in all regions, with localized occurrences of Ca-ferrite, particularly in the edge and outer

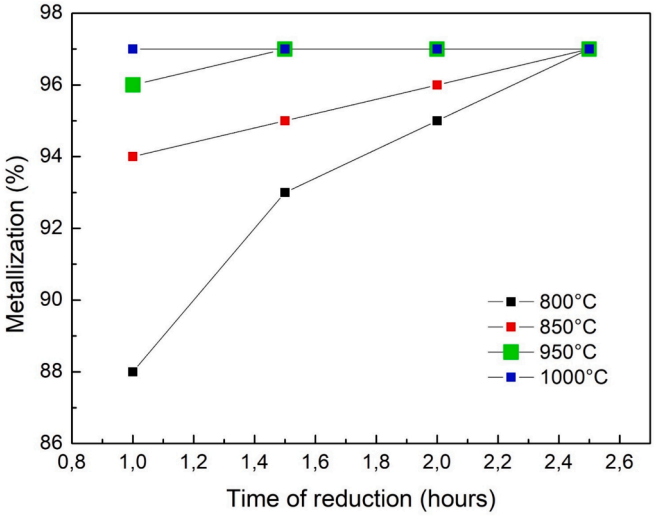


**Fig. 17.** Metallization degree as a function of temperature and time to reduction.

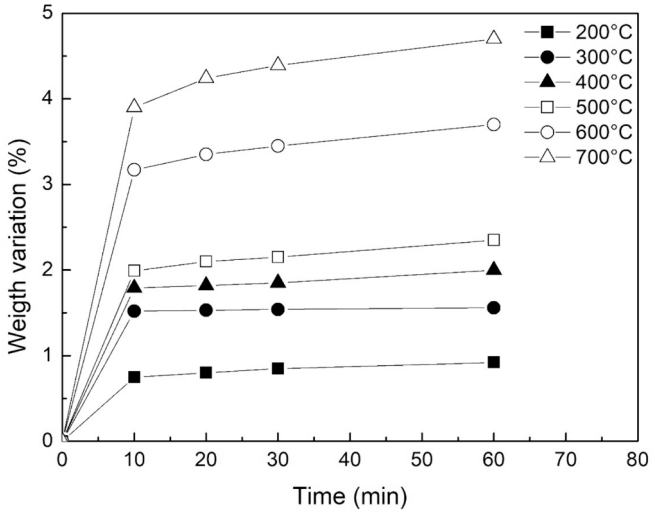


**Fig. 18.** Weight variation of the pellets as a function of temperature and pressure (reoxidation curves refer to the pellets with larger diameter).

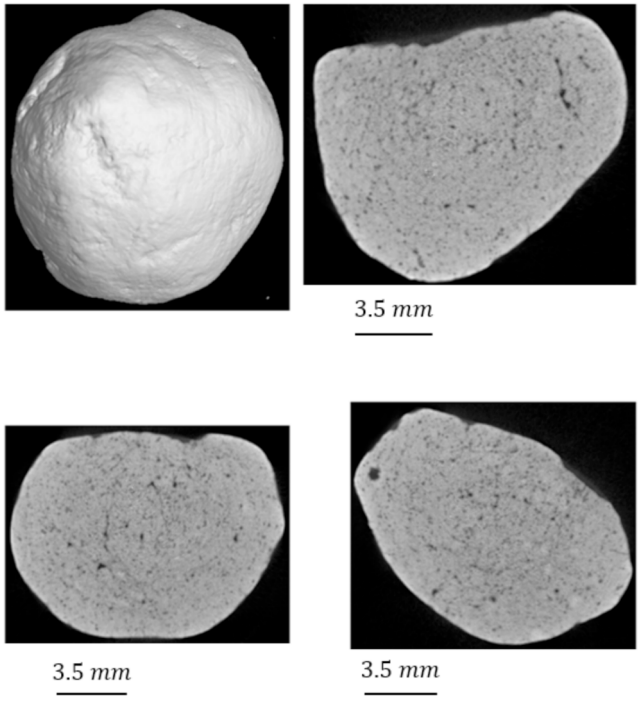


**Fig. 19.** Aspect of the pellets (medium size) after reoxidation at 700 °C for 60 min.

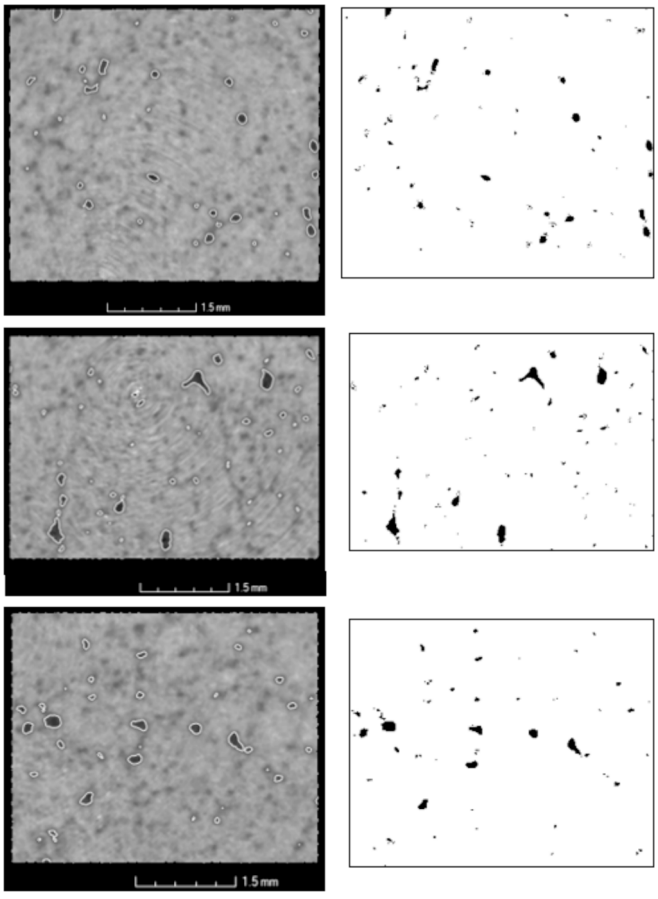


**Fig. 20.** Porosity measurement of the reoxidized pellet.

mantle regions. We have also noted intergranular porosity and medium-sized pores, likely originating from certain inputs. Calcium silicate permeates the gaps between hematite particles.

Hematite is the dominant mineral observed in all regions, with localized occurrences of Ca-ferrite, particularly in the edge and outer mantle regions. Intergranular porosity and medium-sized pores are also present, likely originating from certain inputs or processes. Calcium silicate is found permeating the spaces between hematite particles. After completed metallization the aspect of the pellets microstructure is shown in Fig. 16.

In all regions, it is observed the predominance of metallic Fe. Despite the substantial transformation, it is still possible to identify the contours of the previous oxide phase. The reduced pellet exhibits high porosity, allowing us to distinguish intergranular porosity, which remains from the oxide particles, and intragranular porosity, generated during the transformation of metallic Fe oxide. Furthermore, various tests were performed to assess the metallization and reducibility of numerous pellets, each weighing hundreds of grams. The rate of metallization increases as the reactor temperature rises, as illustrated in Fig. 17.

When considering the time required for reduction, it becomes evident that the primary influencing factor is the pellet diameter, followed by pellet density, both of which have a direct correlation. Gas temperature and pore size exhibit an inverse correlation with the reduction time. Interestingly, pores' tortuosity appears to have a lesser impact, showing a direct correlation with the reduction time.

The effect of pellet size on the reduction process is influenced by pellet density. For high-density pellets, the impact of pellet diameter decreases, while the opposite is observed for larger particles, where density has a reduced effect (Scharm et al., 2022). Consequently, the time required to achieve reduction is primarily dependent on the size of surface pores. Larger pores lead to faster pellet reduction. However, this relationship is also influenced by pellet density, as an increase in pellet density results in a longer time to reduction. Additionally, when considering individual pores, pore tortuosity plays a role in the time to reduction. At the same pore size, an increase in tortuosity leads to a longer time to reduction. In the case of high-density pellets, reduction reactions occur in a stepwise manner and can be modeled through a shrinking core description. This leads to longer reduction times, which are directly proportional to pellet size. Conversely, low-density pellets allow for rapid gas diffusion, resulting in significantly shorter reduction times. Thus, the time required for reduction is shorter for low-density pellets, particularly when they also have intermediate-sized surface pores (Pal et al., 2017; Nguyen et al., 2021). The tortuosity of pores inside the pellets further influences the time to reduction, with increased tortuosity, decreased porosity (increased density), and smaller pore dimensions all leading to longer reduction times.

The behavior of pellet reduction in hydrogen direct reduction is influenced by a hierarchy of phenomena that span from macroscopic scales to atomic ones. These phenomena are contingent on kinetic behavior and encompass heat and mass transfer, involving catalytic processes, diffusion, dissociation, and charge transfer. The intricate nonlinear interactions between these phenomena necessitate the use of diverse characterization and modeling tools for comprehensive understanding. The effects of reduction degree, temperature, and atmosphere on the swelling behavior of pellets have been studied thoroughly under typical hydrogen-based shaft furnaces. Computational analysis of hydrogen reduction of iron oxide pellets in a shaft furnace process has also been conducted. The model relies on a detailed description of the main physical–chemical and thermal phenomena, using a multi-scale approach. The calculated results reveal the detailed behavior of the reduction process, which is likely to reduce CO2 emissions from the steel industry.

The behavior of pellet reduction is influenced by macroscopic transport and diffusion of gases, which play varying roles at different scales within the process. These roles are intimately linked to the microstructure and chemical-physical properties of the pellets. At the

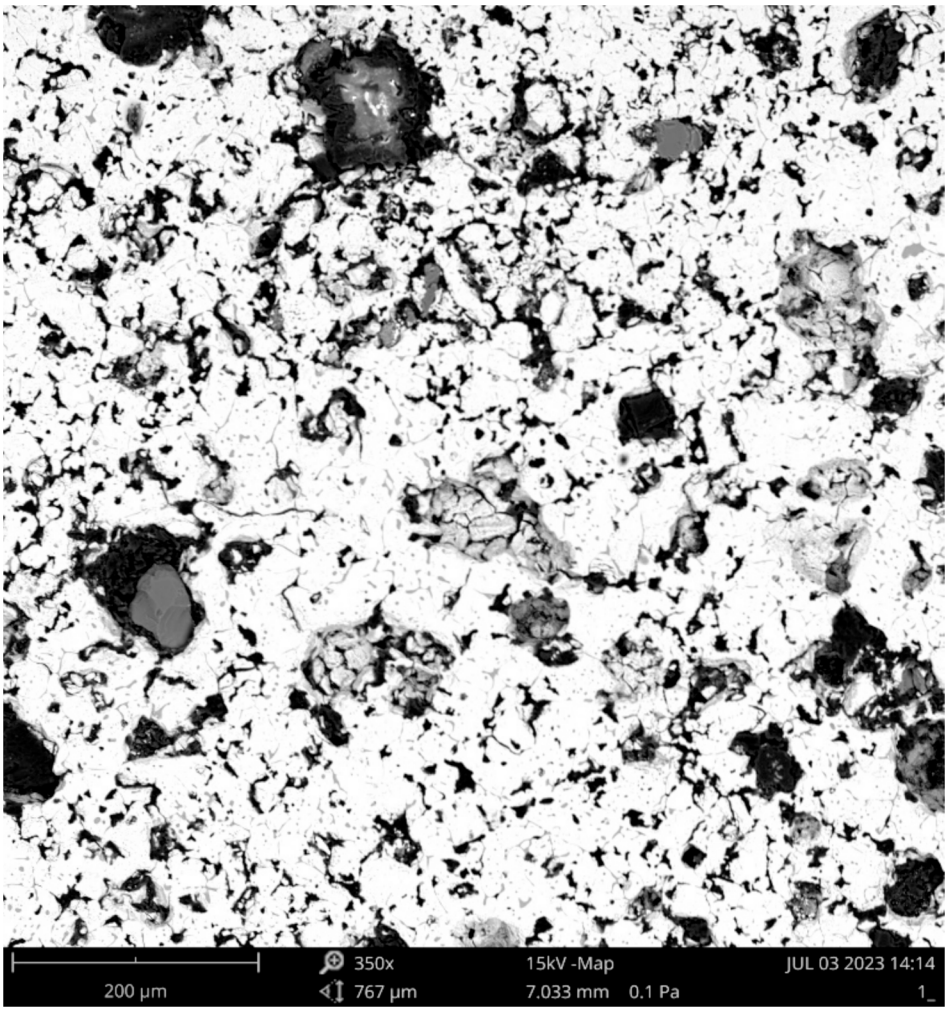


**Fig. 21.** SEM microstructure of the pellet after reoxidation.

microscale, process kinetics are shaped by phenomena occurring at both micro and atomic scales due to the transformations involving different oxides, crystal defects, and local compositions. Several macroscopic studies exist on the reduction of iron oxide exposed to different gas mixtures, and these studies play a critical role in the reduction process itself (Chai et al., 2022; Fan et al., 2021; Chai et al., 2022). The reduction swelling process of pellets prepared from the Bayan Obo iron ore concentrate has been explored based on the iron oxide reduction. The reducing reactions of different composite pellets were mainly controlled by gasification diffusion. The reduction rates can be described by the kinetic analysis. The effect of iron ore pellet size on metallurgical properties has also been studied, and it was found that the size distribution is important for the permeability of the ore burden layers in the furnace. The swelling of pellets characterizes the vulnerability to change in volume during reduction and is tested to ensure that the volume increase during reduction does not exceed a set maximum.

The reduction process of iron ore pellets is influenced by various factors, including processing conditions, pellet composition, density, porosity, and size. Tortuosity plays a significant role in reduction kinetics, as highly tortuous pellets exhibit reduced reaction kinetics, both temporally and spatially. As tortuosity increases, the kinetic constants decrease, as fewer hydrogen atoms interact with the material bulk under similar conditions of pressure, temperature, and mass transfer. Precisely, highly tortuous pellets exhibit reduced reaction kinetics, both temporally and spatially. Consequently, the degree of metallization of pellets is dependent on temperature, followed by tortuosity, gas temperature, pellet diameter, and, finally, density and pore size. The most influential parameter governing metallization behavior is the reduction temperature. The degree of metallization is dependent on temperature, followed by tortuosity, gas temperature, pellet diameter, and, finally, density and pore size (Iljana et al., 2022; Sadeghi et al., 2024; Cavaliere et al., 2024; Cavaliere et al., 2024).

Subsequent to complete metallization, the pellets underwent reheating at various temperatures to assess their reoxidation behavior, and the results are depicted in Fig. 18.

Oxidation initially occurs at low temperatures through the reaction of metallic iron with humidity in the air:

$$2Fe + H_2O + 3O \leftrightarrow 2FeOOH$$

These reactions are very exothermic and release an amount of heat that provides enough energy to enable the other oxidation reactions:

$$3Fe + 2O_2 \leftrightarrow Fe_3O_4$$

$$2Fe_3O_4 + \frac{1}{2}O_2 \leftrightarrow 2Fe_2O_3$$

$$Fe + \frac{1}{2}O_2 \leftrightarrow FeO$$

The last reaction takes place above 570 °C.

The oxidation process of iron sponge is characterized by three distinct stages, each with a different rate of oxidation. The first stage is the rapid initial stage, where the oxidation rate is high, and chemical

reactions at the interfaces play a dominant role. The second stage is the intermediate stage, where the oxidation rate gradually decreases, and diffusion in the solid state becomes the controlling mechanism. The final stage is marked by a low and almost constant rate of oxidation, where solid-state diffusion with the formation of cavities at the interfaces between the oxide film and the metallic iron grains is the predominant mechanism. The observed behavior is influenced by several factors, including the rapid reduction in porosity during oxidation, which limits the diffusion of the oxidizing gas and the reactivity of the particle surfaces. As a result, the rate of oxidation decreases, and non-porous oxide layers block further oxidation. This complex interplay of mechanisms leads to the observed stages in the oxidation process. The oxidation process is exothermic, leading to a significant increase in the temperature of the iron sponge as heat is released. The behavior of the oxidation process is influenced by several factors, including processing conditions, porosity, and the reactivity of the particle surfaces.

The microtomography aspect of the medium size pellet after reoxidation at 700 °C for 60 min is shown in Fig. 19.

The porosity aspect after reoxidation is shown in Fig. 20.

The SEM microstructure and the compositional map of the medium size pellets after reoxidation at 700 °C for 60 min is shown in Fig. 21.

The analysis of the reoxidized pellets reveals a complex transformation process. Metallic iron (Fe) dominates in the reoxidized pellets, indicating that a substantial portion of the initially reduced iron remains in its metallic state after reoxidation. Minor phases such as silicates and Ca-ferrites are also present, suggesting the existence of impurities or secondary compounds. The pellets exhibit a zoned structure, with the core primarily transforming into hematite, an iron oxide. At the outer mantle, a narrow magnetite-wustite transition zone is observed, mainly in the region containing metallic iron. Importantly, the Fe-metallic phase remains preserved in the core. Additionally, some regions show a coexistence of magnetite and wustite without clear boundaries. This complex behavior underscores the intricate nature of iron oxide phase transformations during reoxidation, providing valuable insights for understanding the properties and applications of these materials.

## 4. Conclusions

In view of the extensive research performed in this study, many important conclusions can be drawn. The careful microtomographic studies performed on individual pellets, both before and after direct hydrogen reduction, have provided a comprehensive mapping of the porosity evolution in these materials. It is evident that porosity, pore size, and pore tortuosity vary as a function of specific processing parameters, especially with temperature variations and a gas pressure of 8 bar. These variations in porosity properties have profound effects on the kinetics of the reduction process, as the rate of porosity change is strongly influenced by temperature conditions. Consequently, this leads to variations in diffusion dynamics and gas–solid interactions throughout the reduction process. Multi-pellet reduction experiments have shown that satisfactory metallization occurs at temperatures above 850 °C. Overall, these comprehensive findings contribute to a deeper understanding of the behavior of iron ore pellets during the production and reduction processes and ultimately provide information for strategies to optimize their performance in industrial applications.

## CRediT authorship contribution statement

**Pasquale Cavaliere:** Conceptualization, Data curation, Funding acquisition, Investigation, Methodology, Project administration, Supervision, Validation, Writing – original draft, Writing – review & editing. **Behzad Sadeghi:** Investigation. **Leandro Dijon:** Resources. **Aleksandra Laska:** Data curation, Formal analysis, Investigation. **Damian Koszelow:** Data curation, Formal analysis, Investigation.

## Declaration of competing interest

The authors declare that they have no known competing financial interests or personal relationships that could have appeared to influence the work reported in this paper.

## Data availability

Data will be made available on request.

## Acknowledgments

Authors would like to thank the Italian Ministry for University and Research (MUR) for the fundings provided under the Grant “Low environmental impact fuels for metallurgical industries- 2022P3PJXN”.

## Appendix A. Supplementary data

Supplementary data to this article can be found online at https://doi.org/10.1016/j.mineng.2024.108746.

## References

Ali, M.L., Fradet, Q., Riedel, U., 2022. Kinetic Mechanism development for the direct reduction of single hematite pellets in $H_2$/CO atmospheres. Steel Res. Int. 93 (12), 2200043. https://doi.org/10.1002/srin.202200043.

Anameric, B., Kawatra, K., 2007. Properties and features of direct reduced iron. Miner. Proc. Extract. Metall. Rev. 28 (1), 59–116. https://doi.org/10.1080/08827500600835576.

Augusto, K.S., Alves, H.D.L., Mauricio, M.H.d.P., Paciornik, S. 3D characterization of iron ore pellets by X-ray microCT. *Image Analysis & Stereology,* 14th International Congress for Stereology and Image Analysis Liège, (2015) July 7-10.

Ba, Y., Mianroodi, J.R., Ma, Y., Silva, A.K.D., Svendsen, B., Raabe, D., 2022. Chemo-mechanical phase-field modeling of iron oxide reduction with hydrogen. Acta Mater. 231, 117899 https://doi.org/10.1016/j.actamat.2022.117899.

Bersenev, I.S., Vokhmyakova, I.S., Borodin, A.V., Pigarev, S.P., Sivkov, O.G., Zagainov, S. A., 2022. Structure and metallurgical properties formation of semireduced pellets. Steel Transl. 52, 331–336. https://doi.org/10.3103/S0967091222030160.

Bezerra, E.T.V., Augusto, K.S., Paciornik, S., 2020. Discrimination of pores and cracks in iron ore pellets using deep learning neural networks. REM, Int. Eng. J. 73 (2) https://doi.org/10.1590/0370-44672019730119.

Biswas, C., Swarnakar, A., Majumder, A., 2023. Utilization of micro-fines in sinter making and its implications on bed permeability and sinter quality. Ironmak. Steelmak. https://doi.org/10.1080/03019233.2022.2163532.

Cavaliere, P., Perrone, A., Marsano, D., 2023. Critical analysis of variable atmosphere gaseous reduction of iron oxides pellets. Ironmak. Steelmak. https://doi.org/10.1080/03019233.2023.2194732.

Cavaliere, P., Perrone, A., Marsano, D., Primavera, V., 2023. Hydrogen-based direct reduction of iron oxides pellets modeling. Steel Res. Int. 94 (6), 2200791. https://doi.org/10.1002/srin.202200791.

Cavaliere, P., Perrone, A., Marsano, D., 2023. Effect of reducing atmosphere on the direct reduction of iron oxides pellets. Powder Technol. 426, 118650 https://doi.org/10.1016/j.powtec.2023.118650.

Cavaliere, P., Perrone, A., Dijon, L., Laska, A., Koszelow, D., 2024. Direct reduction of pellets through hydrogen: Experimental and model behaviour. Int. J. Hydrogen Energy 49C, 1444–1460. https://doi.org/10.1016/j.ijhydene.2023.11.040.

Cavaliere, P., Dijon, L., Laska, A., Koszelow, D., 2024. Hydrogen direct reduction and reoxidation behaviour of high-grade pellets. Int. J. Hydrogen Energy 49C, 1235–1254. https://doi.org/10.1016/j.ijhydene.2023.08.254.

Cavaliere, P. (2019). Blast Furnace: Most Efficient Technologies for Greenhouse Emissions Abatement. In: Clean Ironmaking and Steelmaking Processes. Springer, Cham. 10.1007/978-3-030-21209-4_4.

Cavaliere, P. (2019). Direct Reduced Iron: Most Efficient Technologies for Greenhouse Emissions Abatement. In: Clean Ironmaking and Steelmaking Processes. Springer, Cham. 10.1007/978-3-030-21209-4_8.

Cavaliere, P. (2019). Sintering: Most Efficient Technologies for Greenhouse Emissions Abatement. In: Clean Ironmaking and Steelmaking Processes. Springer, Cham. 10.1007/978-3-030-21209-4_3.

Chai, Y., Fan, Y., Gao, X., Luo, G.P., Wang, Y.-C., An, S., Liu, J., 2022. Effect of basicity on the reduction swelling performance of pellets prepared from Bayan obo iron ore concentrate based on microscopic characterization. Crystals.

Chai, Y., Fan, Y., Li, Z., Wu, J., Zhang, Y., Wang, Y.-C., Luo, G.P., An, S., 2022. Kinetics of reduction in stages of pellets prepared from the bayan obo iron ore concentrate. ACS Omega 7, 7759–7768.

El-Zoka, A.A., Stephenson, L.T., Kim, S.-H., Gault, B., Raabe, D., 2023. The fate of water in hydrogen-based iron oxide reduction. Adv. Sci. https://doi.org/10.1002/advs.202300626.

Fan, Y., Zhang, Y., Li, Z., Chai, Y., Wang, Y.-C., Luo, G.P., An, S., 2021. Mechanism on reduction swelling of pellets prepared from Bayan Obo iron ore concentrate. Ironmak. Steelmak. 48, 1158–1168.
Gautam, S., Cole, D.R., 2022. Effects of pore connectivity and tortuosity on the dynamics of fluids confined in sub-nanometer pores. PCCP 24, 11836–11847. https://doi.org/10.1039/D1CP04955K.
Ghadi, A.Z., Valipour, M.S., Biglari, M., 2016. Mathematical modelling of wustite pellet reduction: grain model in comparison with USCM. Ironmak. Steelmak. 43 (6), 418–425. https://doi.org/10.1080/03019233.2015.1135578.
Ghadi, A.Z., Radfar, N., Valipour, M.S., Sohn, H.Y., 2023. A review on the modeling of direct reduction of iron oxides in gas-based shaft furnaces. Steel Res. Int. 94 (6), 2200742. https://doi.org/10.1002/srin.202200742.
Hamadeh, H., Mirgaux, O., Patisson, F., 2018. Detailed modeling of the direct reduction of iron ore in a shaft furnace. Materials 11 (10), 1865. https://doi.org/10.3390/ma11101865.
Huang, Z., Yi, L., Jiang, T., 2012. Mechanisms of strength decrease in the initial reduction of iron ore oxide pellets. Powder Technol. 221, 284–291. https://doi.org/10.1016/j.powtec.2012.01.013.
Ignacio, I.R., Brooks, G., Pownceby, M.I., Rhamdhani, M.A., Rankin, W.J. 2022. Porosity in Iron Ore Sintering, AISTech 2022 — Proceedings of the Iron & Steel Technology Conference 16–18 May 2022, Pittsburgh, Pa., USA. 10.33313/386/215.
Iljana, M., Paananen, T., Mattila, O., Kondrakov, M., Fabritius, T., 2022. Effect of iron ore pellet size on metallurgical properties. Metals 12 (2), 302. https://doi.org/10.3390/met12020302.
Ju, J., Li, Q., Xing, X.D., Jiang, X., Zhao, G., Lu, F., 2023. Effect of high basicity on compressive strength and microstructure of iron ore pellets containing $TiO_2$. Metall. Res. Technol. 120 (3), 306. https://doi.org/10.1051/metal/2023032.
Kim, T., Sohn, I.l., 2023. Effects of $K_2CO_3$ addition on the physicochemical properties of goethite composite pellets with different basicities (CaO/SiO2). J. Mater. Res. Technol. 25, 4595–4608. https://doi.org/10.1016/j.jmrt.2023.06.247.
Korobeinikov, Y., Meshram, A., Harris, C., Kovtun, O., Govro, J., O'Malley, R.J., Volkova, O., Sridhar, S., 2023. Reduction of iron ore pellets using different gas mixtures and temperatures. Steel Res. Int. https://doi.org/10.1002/srin.202300066.
Lei Jie, Zhang Chen, An Jingshu, Kong Yu-qi, he shengping, Long Hongming, Wu Ting, Mechanism Study on Gas-Based Reduction Swelling Behavior of Ultra-High Grade Pellets. Available at SSRN: https://ssrn.com/abstract=4475187 or 10.2139/ssrn.4475187.
Li, J., Liang, Z., Yi, L., Huang, B., Chen, J., Han, H., Huang, Z., 2021. Novel insights into the reoxidation of direct reduced iron (DRI) during ball-mill treatment: A combined experimental and computational study. Appl. Surf. Sci. 552, 149485 https://doi.org/10.1016/j.apsusc.2021.149485.
Li, Z., Qi, Z., Zhang, L., Guo, M., Liang, D., Dong, Q., 2023. Numerical simulation of $H_2$-intensive shaft furnace direct reduction process. J. Clean. Prod. 409, 137059 https://doi.org/10.1016/j.jclepro.2023.137059.
Ljung, Anna-Lena. "Modeling drying of iron ore pellets." PhD diss., Luleå tekniska universitet, 2010.
Lyu, B., Wang, G., Xie, S., 2023. Effect of hydrogen-rich atmosphere on the reduction behavior and kinetics of iron-ore pellets under non-isothermal conditions. JOM 75, 1540–1550. https://doi.org/10.1007/s11837-022-05693-3.
Ma, K., Deng, J., Wang, G., Zhou, Q.i., Jian, Xu., 2021. Utilization and impacts of hydrogen in the ironmaking processes: A review from lab-scale basics to industrial practices. Int. J. Hydrogen Energy 46 (52), 26646–26664. https://doi.org/10.1016/j.ijhydene.2021.05.095.
Man, Y., Feng, J., 2016. Effect of gas composition on reduction behavior in red mud and iron ore pellets. Powder Technol. 301, 674–678. https://doi.org/10.1016/j.powtec.2016.06.013.
Meshram, A., Govro, J., OMalley, R.J., Sridhar, S., Korobeinikov, Y., 2022. Modeling isothermal reduction of iron ore pellet using finite element analysis method. Exp. Validat. Met. 12 (12), 2026. https://doi.org/10.3390/met12122026.
Metolina, P., de Andrade, R.S., Ramos, B., Guardani, R., 2023. Hydrogen direct reduction ironmaking process for zero $CO_2$ emission: A study on the effect of particle properties changes during the multiple non-catalytic gas-solid reactions. Miner. Eng. 201, 108188 https://doi.org/10.1016/j.mineng.2023.108188.
Mishra, S., 2020. Review on reduction kinetics of iron ore-coal composite pellet in alternative and sustainable ironmaking. J. Sustain. Metall. 6, 541–556. https://doi.org/10.1007/s40831-020-00299-y.
Mohammad, S., Patra, S., Harichandan, B., 2023. Reductants in iron ore sintering: A critical review. Fuel 332 (2), 126194. https://doi.org/10.1016/j.fuel.2022.126194.
Nguyen, C.-S., Nguyen, T.-H., Nguyen, S.-L., Bui, A.-H., 2021. Study on the reducibility of iron ore pellets at high temperature. Viet. J. Sci. Technol. Eng. 63 (4), 3–7. https://doi.org/10.31276/VJSTE.63(4).03-07.
Nie, H., Qi, B., Li, Y., Qiu, D., Wei, H., Hammam, A., Ahmed, A., Yaowei, Yu., 2023. Structure analysis of pellets with different reduction degrees using X-ray micro-computed tomography. Steel Res. Int. 94 (1), 2200241. https://doi.org/10.1002/srin.202200241.
Nurdiawati, A., Zaini, I.N., Wei, W., Gyllenram, R., Yang, W., Samuelsson, P., 2023. Towards fossil-free steel: Life cycle assessment of biosyngas-based direct reduced iron (DRI) production process. J. Clean. Prod. 393, 136262 https://doi.org/10.1016/j.jclepro.2023.136262.
Pal, J., Ghoari, S., Ammasi, A., Hota, S.K., Koranne, V.M., Venugopalan, T., 2017. Improving reducibility of iron ore pellets by optimization of physical parameters. J. Min. Metall. Sect. B-Metall. 53 (1), 37–46. https://doi.org/10.2298/JMMB151206014P.
Pfeiffer, A., Ernst, D., Zheng, H., Wimmer, G., Schenk, J., 2023. The behavior of direct reduced iron in the electric arc furnace hotspot. Metals 13 (5), 978. https://doi.org/10.3390/met13050978.
Rao, N.D., Chakraborty, D.P., Vishal Shukla, Neeraj Kumar. 2023. Iron ore beneficiation: an overview, Mineral Processing-Beneficiation Operations and Process Optimization Through Modeling pp. 55-77. 10.1016/B978-0-12-823149-4.00003-X.
Reddy, A.L.S.B., Sahoo, S.K., Kumar, M., 2023. Studies on characterization of properties of low-grade hematite iron ores and their fired pellets. Ironmak. Steelmak. https://doi.org/10.1080/03019233.2023.2180930.
Rukini, A., Rhamdhani, M.A., Brooks, G.A., 2022. Metals Production and metal oxides reduction using hydrogen: A review. J. Sustain. Metall. 8, 1–24. https://doi.org/10.1007/s40831-021-00486-5.
Sadeghi, B., Cavaliere, P., Bayat, M., Esfahani, N.E., Laska, A., Koszelow, D., 2024. Experimental study and numerical simulation on porosity dependent direct reducibility of high-grade iron oxide pellets in hydrogen. Int. J. Hydrogen Energy 69, 586–607. https://doi.org/10.1016/j.ijhydene.2024.05.050.
Scharm, C., Küster, F., Laabs, M., Huang, Q., Volkova, O., Reinmöller, M., Guhl, S., Meyer, B., 2022. Direct reduction of iron ore pellets by $H_2$ and CO: In-situ investigation of the structural transformation and reduction progression caused by atmosphere and temperature. Miner. Eng. 180, 107459 https://doi.org/10.1016/j.mineng.2022.107459.
Shen, Z., Sun, S., Jianliang, Xu., Liang, Q., Liu, H., 2023. Experimental and modeling study on reduction and heat transfer characteristics of single iron ore pellet in $H_2$/CO atmospheres. ISIJ Int. 63 (1), 42–53. https://doi.org/10.2355/isijinternational.ISIJINT-2022-280.
Singh, A.K., Kumar, A., Kumar, S., Mishra, B., Biswajit, Dishwar, R.K., Mandal, A.K., Rao, L.S., Sinha, O.P., 2022. Direct reduction of fluxed iron ore pellets made from coarse iron ore particles. Can. Met. Quat. 61 (4), 475–482. https://doi.org/10.1080/00084433.2022.2045530.
Singh, A.K., Sinha, O.P., Singh, R., 2023. Reduction behavior and kinetics of iron ore-charcoal composite pellets for sustainable ironmaking. Metall. Mater. Trans. B 54, 823–832. https://doi.org/10.1007/s11663-023-02729-0.
Sundberg, R. 2021. Reduction of iron oxides with hydrogen, Master Degree Thesis, Abo Akademy University.
Tang, K., Wang, Y.D., Niu, Y., Honeyands, T.A., O'Dea, D., Mostaghimi, P., Armstrong, R. T., Knackstedt, M., 2023. Particle classification of iron ore sinter green bed mixtures by 3D X-ray microcomputed tomography and machine learning. Powder Technol. 415, 118151 https://doi.org/10.1016/j.powtec.2022.118151.
Wei, W., Zheng, H., Runsheng, Xu., Fenglou, Wu., Chen, W., Jia, B., Xue, Z., 2019. Characterization of the mineral phases of the iron ore pellet via 3D reconstruction using serial sectioning. Metall. Res. Technol. 116, 117. https://doi.org/10.1051/metal/2018056.
Yazir, D., Sahin, B., Alkac, M., 2021. Selection of an inert gas system for the transportation of direct reduced iron. Mathem. Prob. Eng. 8529724. https://doi.org/10.1155/2021/8529724.
Yi, L., Huang, Z., Jiang, T., 2013. Sticking of iron ore pellets during reduction with hydrogen and carbon monoxide mixtures: Behavior and mechanism. Powder Technol. 235, 1001–1007. https://doi.org/10.1016/j.powtec.2012.11.043.
Zhang, S., Jiang, D., Wang, Z., Zong, Y., Zhang, J., Wang, F., Si, R., Zhang, S., Zhou, X., Pang, J., 2023. Sulfur migration behavior in sintering and pelletizing processes: A review. Steel Res. Int. https://doi.org/10.1002/srin.202200904.
Zhang, Z., Wong, J.J., Scott, S.A., Fennell, P.S., 2023. Spouted fluidised bed reactor for kinetic measurements of the reduction of $Fe_2O_3$ in a CO/$CO_2$ atmosphere part II: An extended random pore model for solid-state diffusion. Chem. Eng. Res. Des. 194, 597–609. https://doi.org/10.1016/j.cherd.2023.04.054.
Zheng, Z., Li, Y., Guo, Q., Zhang, L., Qi, T., 2023. Promoting the reduction reactivity of magnetite by introducing trace-K-ions in hydrogen direct reduction. Int. J. Hydrogen Energy 48 (48), 18177–18186. https://doi.org/10.1016/j.ijhydene.2023.01.268.